

# 1

## X-ray polarization from accreting white dwarfs and associated systems

Kinwah Wu (University College London)

Aimee McNamara (University of Sydney)

Zdenka Kuncic (University of Sydney)

### Abstract

We present our results of Monte-Carlo simulations of polarized Compton X-rays from magnetic cataclysmic variables, with realistic density, temperature and velocity structures in the accretion flow. Our study has shown that the X-ray linear polarization may reach about 8% for systems with high accretion rates viewed at a high viewing inclination angle. This value is roughly twice the maximum value obtained by previous studies which assumed a cold, static emission region with a uniform density. We also investigate the X-ray polarization properties of ultra-compact double-degenerate binaries for the unipolar-inductor and direct-impact accretor models. Our study has shown negligible X-ray polarization for the unipolar-induction model. However, the direct-impact accretor model may give X-ray polarization levels similar to that predicted for the magnetic cataclysmic variables.

### 1.1 Introduction

Magnetic cataclysmic variables (mCVs) and Ultra-compact double degenerate binaries (UCDs) are potential X-ray polarization sources. mCVs contain a magnetic white dwarf accreting material from a low-mass, Roche-lobe filling companion star. There are two major types: (i) the AM Herculis binaries (AM Hers, also known as polars) and (ii) the intermediate polars (IPs) (see (13)). In AM Hers, the white-dwarf magnetic field ( $B \sim 10^7 - 10^8$  G) is strong enough to lock the whole system into synchronous rotation. It also prohibits the formation of an accretion disk, and the accretion flow is channelled by the magnetic field into the magnetic polar regions of the white dwarf. The white dwarf in an IP has a weaker magnetic field ( $B \sim 10^6$  G). The white-dwarf magnetosphere truncates the inner part of the accretion disk, and the material flow is channelled by the magnetic field from the

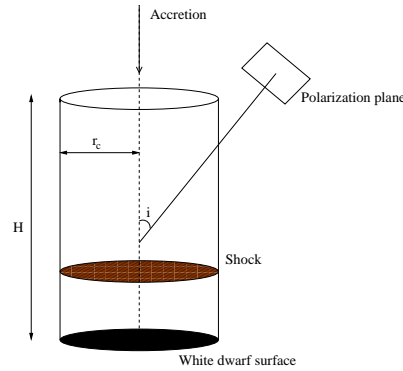


Fig. 1.1. An illustration of the emission region in mCVs where the polarized X-rays are generated. The accretion column has a circular cross-section, with a radius  $r_c$ . Compton scatterings occur within a height  $H$  from the white-dwarf surface.

inner disk rim to the white-dwarf surface. For both AM Her and IP, the supersonic accretion flow becomes subsonic abruptly near the white dwarf surface, thereby forming an accretion shock. The shock heats up the accreting matter to keV temperature, and X-rays and optical/IR radiation are emitted from the shock-heated gas as it cools and settles onto the white-dwarf surface (see e.g. (16)).

A UCD consists of two white dwarfs revolving around each other in a very tight orbit (which has a linear size of Jupiter). There are debates on what mechanisms generate the X-rays in UCDs. The leading models are the unipolar-inductor (UI) model (19) and the direct-impact accretor (DIA) model (6). In the UI model, the UCD orbital dynamics are determined jointly by magnetic interaction and gravitational radiation. Magnetic induction similar to that in Jupiter and Io sets up an electric current circuit across the binary. The electrical dissipation at the foot-points of magnetic field lines connecting the two white dwarfs heats up the white-dwarf atmosphere. Because of the convergent field configuration, small hot spots are formed at the surface of the magnetic white dwarf and emit X-rays. In the DIA model, the X-rays are accretion powered as in conventional binary X-ray sources. The close proximity between the two white dwarfs creates a strong tidal interaction and this prohibit the formation of an accretion disk. Mass transfer between the two stars is instead facilitated by a dense material stream. X-rays are emitted from a hot spot, where the accretion stream impacts onto the white-dwarf surface. The accretion configuration of the DIA model is somewhat similar to that of AM Hers.

The optical/IR emission from AM Hers is strongly polarized. The circular polarization can be as high as several ten percents (17). The optical/IR polarization is generated by a thermal cyclotron process (1), where energetic electrons in the shock-heated plasma gyrate around the magnetic field. Optical/IR circular polarization has been observed in several IPs (see (11)), but it is much weaker than that of the AM Hers. The origin of the polarization is believed to be the same as that of AM Hers. In the UI model, UCDs are predicted to be strong sources of electron-cyclotron masers (14; 15). The masers are generated through a loss-cone or a shell instability (see (9)) developed in the electron population when the charged particles stream along the converging magnetic field lines near the polar regions of the magnetic white dwarf. The masers are characterized by a high brightness temperature and almost 100% circular polarization.

Polarization in the low-energy emission of mCVs is produced by processes involving gyration of electron around a magnetic field. Their X-ray polarization is, however, unrelated to magnetic plasma processes. Instead it is due to scattering, where unpolarized thermal X-ray photons emitted from the shock-heated region are scattered by the electrons that precipitate onto the white dwarf. In this article we show the results of our calculations of X-ray polarization in mCVs and discuss briefly the astrophysical implications of our findings. We also show some preliminary results from our study of X-ray polarization in ultra-compact double degenerate binaries.

## 1.2 Results and Discussions

### 1.2.1 *X-ray polarization in magnetic cataclysmic variables*

The geometrical setup in our calculations is shown in Figure 1.1. The density, temperature and velocity structure in the post-shock emission region is determined by the hydrodynamics model given in (18; 20). Unless otherwise stated, thermal free-free emission is the dominant cooling process. We consider a Monte-Carlo approach to simulate the Compton scattering events and the transport of the polarized X-ray photons in the accretion column. A non-linear algorithm based on (2; 3) is used to determine the photon mean-free path and the scattering probability. The scattering variables are determined following the prescriptions described in (12). The polarizations are calculated using the Klein-Nishina cross section and the formulation for photon-electron scattering given in (4; 5). The polarized photons that escape from the accretion column are binned according to their energy-momentum and summed to give the spectral polarization at specific intervals of viewing

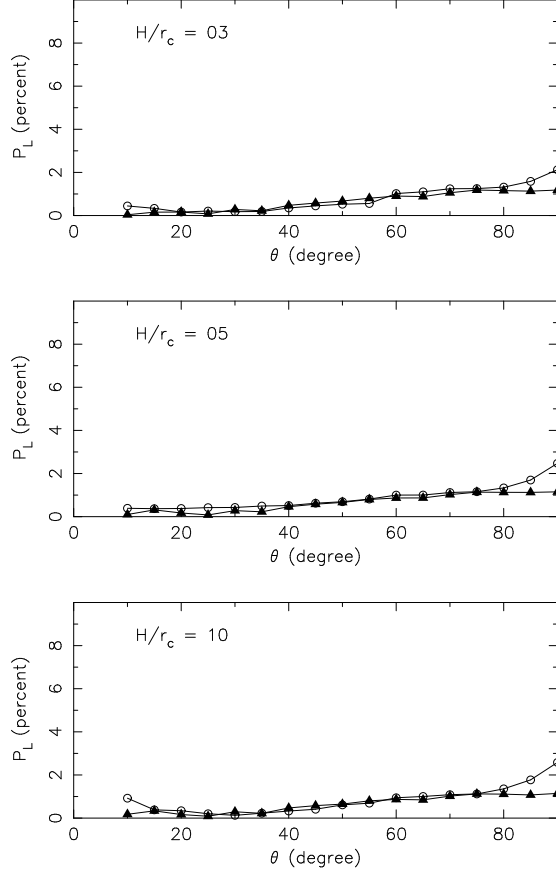


Fig. 1.2. Linear polarization  $P_L$  of X-rays as a function of the viewing inclination angle  $\theta$  for accretion onto magnetic white dwarfs with masses of  $1 M_\odot$ . Filled triangles correspond to the cases with a specific accretion rate  $\dot{m} = 1 \text{ g cm}^{-2} \text{ s}^{-1}$ ; and open circles correspond to the case with 10 times higher specific accretion rates. The Thomson scattering optical depths across the accretion shock are  $\tau = 0.04$  and  $0.3$  respectively. The  $H/r_c$  ratios are 3, 5 and 10 (panels from top to bottom).

inclination angles. The formulation, computational algorithms and numerical simulation procedures are presented in detail in (8).

Figures 1.2 and 1.3 show the results of two example simulations. For the case with a  $1.0\text{-}M_\odot$  white dwarf, the maximum value of the linear polarization  $P_L$  is about 1–2%. For the case with a  $0.5\text{-}M_\odot$  white dwarf, the maximum  $P_L$  may reach about 8% for viewing angle  $\theta \approx 90^\circ$ . The polarization increases slightly with  $\theta$  for low specific accretion rates ( $\dot{m} \sim 1 \text{ g cm}^{-2} \text{ s}^{-1}$ ).

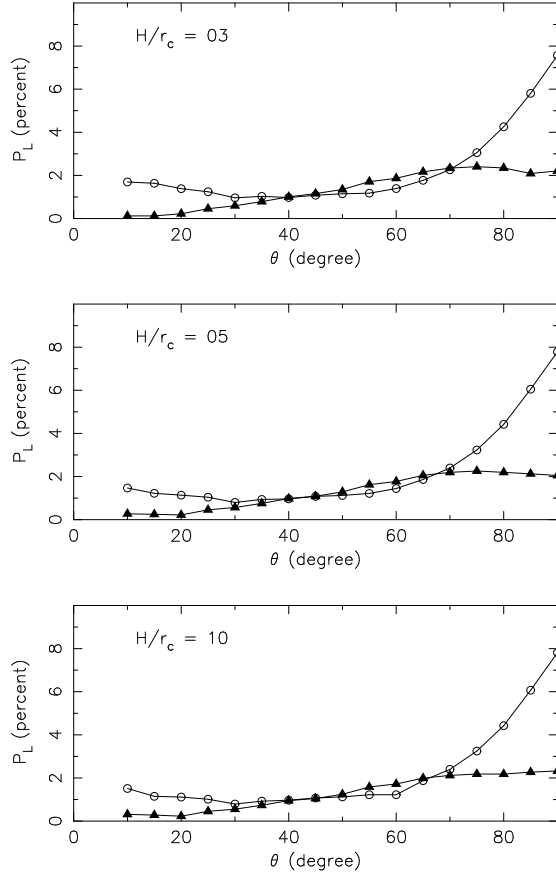


Fig. 1.3. Same as Figure 1.2 for white dwarfs with masses of  $0.5 M_{\odot}$ . The Thomson scattering optical depths across the accretion shock are  $\tau = 0.1$  and  $1.0$  for the cases with low and high specific accretion rates respectively.

However, for sufficiently high  $\dot{m}$  ( $\sim 10 \text{ g cm}^{-2} \text{ s}^{-1}$ ), the polarization could increase substantially at large  $\theta$ .

Figure 1.4 shows a comparison of the polarization from a structured accretion flow and a cold, static and uniform density emission region. For low accretion rates, the cold, static, uniform density emission region underpredicts the linear polarization, especially at large  $\theta$ . For high accretion rates, it overpredicts the polarization for angles below about  $70 - 80^{\circ}$ . The main difference of the two models is that the structured flow model always has a highly dense base region, where most of the scatterings occur, but the static model has a uniform density throughout the scattering region. The

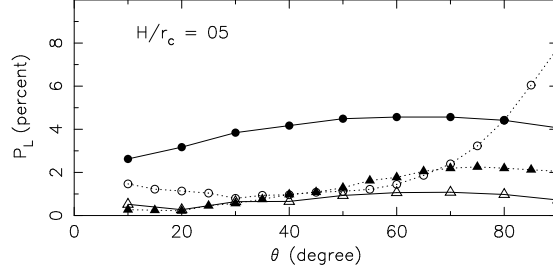


Fig. 1.4. Comparison between the X-ray polarizations predicted by a static, cold emission region with a uniform density (solid lines) and by an emission region with structures determined by the hydrodynamic model of (18) (dotted lines). The parameters of the models are the same as those of the case in the middle panel of Figure 1.3. Triangles correspond to cases with  $\dot{m} = 1 \text{ g cm}^{-2} \text{ s}^{-1}$ ; and circles correspond to cases with  $\dot{m} = 10 \text{ g cm}^{-2} \text{ s}^{-1}$ .

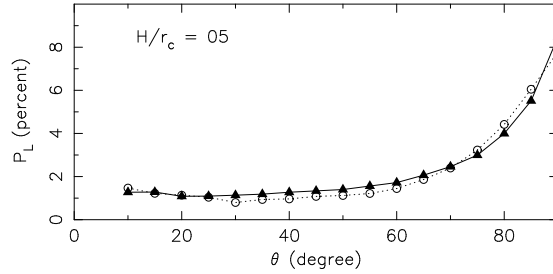


Fig. 1.5. Comparison between X-ray polarizations from mCVs with accretion flows dominated by thermal free-free cooling and by cyclotron cooling. The white-dwarf mass is  $0.5 M_\odot$ , and the specific accretion rate is  $10 \text{ g cm}^{-2} \text{ s}^{-1}$ . The ratios of efficiencies of cyclotron to thermal free-free cooling at the shock  $\epsilon_s = 0$  (open circles) and 10 (filled triangles).

underprediction of the polarization by the uniform model at low  $\dot{m}$  is due to the lack of a dense base layer which gives a substantial scattering optical depth. The overprediction of the polarization by the uniform model at high  $\dot{m}$  is caused by a uniformly high scattering optical depth at all heights above the white-dwarf surface, in contrast to the density drop off with height in the stratified accretion flow.

The high density at the base and rapid density drop off with height are also the reasons why the angle dependence of the polarization is insensitive to the accretion-column aspect ratio in the cases with stratified accretion

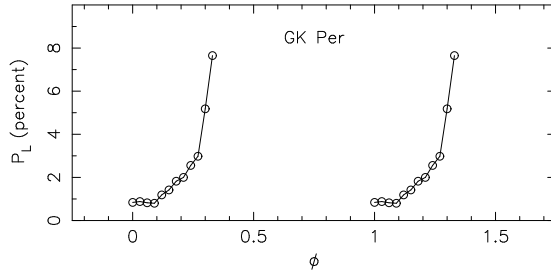


Fig. 1.6. Predicted X-ray linear polarization in the mCV GK Per as a function of the white-dwarf spin phase  $\phi$ . In the simulations the white-dwarf mass is set to be  $0.63 M_{\odot}$  (10), and the specific accretion rate is assumed to be  $10 \text{ g cm}^{-2} \text{ s}^{-1}$ .

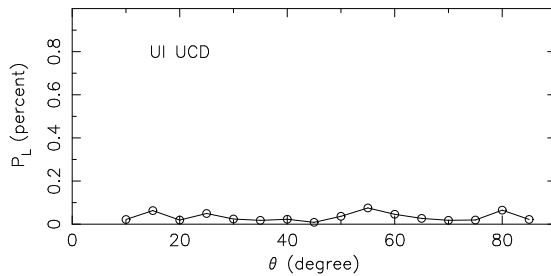


Fig. 1.7. Linear polarization as a function of viewing inclination angle for a UI UCD model. In the model, the bulk Lorentz parameter of the fast streaming electrons  $\Gamma = 10^3$ , the effective Thomson scattering depth across the column  $\tau = 10^{-3}$ . The  $H/r_c$  ratio is 100.

flows. The situation is different for a static, uniform-density scattering region (see (7)), where the effective scattering optical depth depends strongly on the viewing inclination and the aspect ratio of the accretion column. Note the polarization is insensitive to the cyclotron cooling process for the same reason, as scatterings occur mainly in the dense base not the less dense region immediately below the shock (Figure 1.5). Figure 1.6 shows the predicted polarization from a system with the same parameters as those derived for the IP GK Per.

### 1.2.2 X-ray polarization in ultra-compact double degenerates

The accretion geometry of the DIA UCD is similar to that of the AM Hers, except that an accretion shock might not be formed. In terms of Compton

scattering, the model set up would be approximately the same as that of the case with a static, uniform density accretion column. Although the gas has a bulk motion in the accretion column, the relatively slow speed implies that Compton recoil is the dominant effect in the scattering event. As a first approximation the consequence is not much different from that for the case with cold electrons. The polarization is therefore of the order of 1 – 4% (see (7)). Thus, as a rough estimate, a polarization of a few percent would be expected from the DIA UCD model. The UI UCD does not have a dense accretion column. Instead there is a stream of relativistic electrons. The dominant effect is Doppler shift instead of recoil. Moreover, almost all events are head-on as seen by the relativistic electrons. Figure UCD shows our simulation for a model UI UCD. As the scattering optical depth is small, there is no substantial polarization. X-ray polarization can clearly distinguish the DIA and the UI model for UCD, despite the fact that the two models could have very similar X-ray spectral and timing properties.

### References

- [1] Chanmugam, G., Dulk, D.A. (1981). *ApJ*, **244**, 569–578.
- [2] Cullen, J.G. (2001a). PhD Thesis, University of Sydney.
- [3] Cullen, J.G. (2001b). *JCoPh*, **173**, 175–186.
- [4] Heitler, W. (1936). *Quantum Theory of Radiation* (Oxford University Press, Oxford).
- [5] Jauch, J.M., Rohrlich, F. (1980). *The Theory of Photons and Electrons* (Springer-Verlag, Berlin).
- [6] Marsh, T., Steeghs, D. (2002). *MNRAS*, **331**, L7–L11.
- [7] Matt, G. (2004). *MNRAS*, **423**, 495–500.
- [8] McNamara, A.L., Kuncic, Z., Wu, K. (2008). *MNRAS*, **386**, 2167–2172.
- [9] Melrose, D.A., Dulk, D.A. (1982). *ApJ*, **259**, 844–858.
- [10] Morales-Reuda, L., Still, M.D., Roche, P., Wood, J.H., Lockley, J.J. (2002). *MNRAS*, **329**, 597–604.
- [11] Piirola, V., Hakala, P., Coyne, G.V. (1993). *ApJ*, **410**, L107–L110.
- [12] Pozdnyakov, L.A., Sobol, I.M., Sunyaev, R.A. (1983). *Astrophys. Space Phys. Rev.*, **2**, 189–331.
- [13] Warner, B. (1995). *Cataclysmic Variables* (Cambridge University Press, Cambridge).
- [14] Willes, A.J., Wu, K. (2004). *MNRAS*, **348**, 285–296.
- [15] Willes, A.J., Wu, K., Kuncic, Z. (2004). *PASA*, **21**, 248–251.
- [16] Wu, K. (2000). *Space Sci. Rev.*, **93**, 611–649.
- [17] Wu, K., Wickramasinghe, D.T. (1990). *MNRAS*, **246**, 686–698.
- [18] Wu, K., Chanmugam, G., Shaviv, G. (1994). *ApJ*, **426**, 664–668.
- [19] Wu, K., Cropper, M., Ramsay, G., Sekiguchi, K. (2002). *MNRAS*, **331**, 221–227.
- [20] Wu, K., Cropper, M., Ramsay, G., Saxton, C., Bridge, C. (2003). *ChJAS*, **3**, 235–244.